RSC Advances

PAPER

View Article Online
View Journal | View Issue

Cite this: *RSC Adv.*, 2021, **11**, 31526

New *in situ* description of electrodepositing multiple nucleation processes under galvanostatic stimuli†

Yuan Yuan,[a] Gong Luo *[ab] and Ning Li *[a]

Received 28th June 2021
Accepted 9th September 2021

DOI: 10.1039/d1ra04988g

rsc.li/rsc-advances

Chronoamperometry was used to investigate phase transformations at the early stage of electrodeposition under potentiostatic stimuli. Whilst electrodeposition mostly occurs under galvanostatic stimuli, this work provides a new *in situ* description using chronopotentiometry to analyse phase transformations during electrodeposition. With theoretical Ohm's law electro-relationship formula derivation, a non-dimensional plot between $(\Delta E_{min}/\Delta E_T)^2$ and t/t_m was established similar to $(I_t/I_{max})^2$ *vs.* t/t_m in the SH model. The non-dimensional plots were verified by the chronopotentiometry curve during gold electrodeposition. This work provides a new method of investigating phase transformation using chronopotentiometry during electrodeposition.

Introduction

Electrochemical phase transformations have attracted much attention at the early electrodepositing stage in research.[1,2] Most reports have revealed that phase transformations usually occur with three-dimensional nucleation processes.[3,4] In many cases of electrodeposition, the charge-transfer step is controlled by mass-transfer of electrodepositing ions to the growing centres.[3] Obviously, the rate of phase transformation and the number of nuclei formed depend on the stimulant signal, potentiostatic or galvanostatic stimuli. Therefore, the exact relationship between the stimulant signal and the kinetics of the nucleation process should be established.

Early studies describing the growth of nuclei assumed that the transfer of ions to individual nuclei was through two-dimensional growth similar to the Ag deposition process.[5–7] Considering the small size of nuclei, the growth of nuclei would be better described as three-dimensional growth. Three-dimensional cone type growth was assumed at an early stage by Armstrong.[8] Then, different three-dimensional shape growth processes were studied by Bosco and Rangarajan.[9,10] Finally, three-dimensional hemispherical growth was verified as the closest to reality, and a localised spherical diffusion process was assumed.[11] This description of three-dimensional hemispherical growth was subsequently verified by computer simulation.[12] The growth current of single nuclei growth was also confirmed.[13,14]

Based on previous studies, a three-dimensional hemispherical infinite diffusion mass transfer electro-crystallisation model was established by Hills and Scharifker,[4,15,16] called the SH model. The expressions between transient current I and electrodeposition time t under instantaneous nucleation and progressive nucleation are calculated as eqn (1) and (2).

For instantaneous nucleation:

$$I = zFcD^{1/2}/(\pi t)^{1/2}(1 - \exp(-N\pi kDt)), \quad (1)$$

For progressive nucleation:

$$I = zFcD^{1/2}/(\pi t)^{1/2}(1 - \exp(-AN_m\pi KDt^2/2)), \quad (2)$$

where D is the diffusion coefficient, c is the bulk concentration, zF is the molar charge of the electrodepositing species, N is the number of centres instantaneously nucleated per unit area at $t = 0$ and k and K are the numerical condition constants of the experiment, which are $k = (8\pi cM/\rho)^{1/2}$ and $K = \frac{4}{3}(8\pi cM/\rho)^{1/2}$, respectively. For progressive nucleation $N_{(t)} = AN_m t$, where A is the nucleation rate per active site. M and ρ are the molecular weight and density of the deposited material, respectively.

Group non-dimensional plots for instantaneous nucleation and progressive nucleation were calculated as eqn (3) and (4), respectively.

Instantaneous nucleation:

$$\left(\frac{I_t}{I_{max}}\right)^2 = \frac{1.9542}{t/t_m}\{1 - \exp[-1.2564(t/t_m)]\}^2, \quad (3)$$

Progressive nucleation:

[a]School of Chemistry and Chemical Engineering, Harbin Institute of Technology, Harbin 150001, People's Republic of China. E-mail: lininghit@263.net

[b]College of Mechanical and Electrical Engineering, Guangdong University of Petrochemical Technology, Maoming, 525000, People's Republic of China. E-mail: xiaoluo412144143@163.com

† Electronic supplementary information (ESI) available. See DOI: 10.1039/d1ra04988g

$$\left(\frac{I}{I_{max}}\right)^2 = \frac{1.2254}{t/t_m}\left\{1-\exp\left[-2.3367(t/t_m)^2\right]\right\}^2, \quad (4)$$

where I_{max} and t_m are the respective current maxima and the corresponding time for instantaneous and progressive nucleation.

The non-dimensional plots under potentiostatic stimuli have been widely researched and applied in metal electrodepositing nucleation.[17–20] Many studies used non-dimensional plots to analyse the nucleation process under galvanostatic stimuli, such as Au,[21,22] Ag,[23] Cu,[24] Sn,[25] Zn-Ni[26] and Sn–Co alloy.[27] With the wide use of the SH model, further amendments were introduced for this model. Scharifer[28] amended the equation using extra electrochemical reaction. Mostany J.[29] amended the equation using a variable nuclei quantity, named as 'α'. Heerman L.[30] introduced the Dawson integral to amend the SH model using parameter 'Φ'. Altimari P.[31] proposed a mixed kinetic-diffusion control model to describe electrodeposition.

In our early work, we established a limited-diffusion theory model based on a single hemispherical nucleation process reported in the SH model and Brownian motion explained by D'Ajello P. C. T. and Munford M. L.[32] The limited-diffusion theory model provides a detailed description of multiple nucleation processes during electrodeposition. The model has reproduced the potentiostatic current transient curves obtained from gold electrodeposition.[33]

Only a few studies have mentioned the nucleation process under galvanostatic stimuli.[34] However, electrodeposition mostly occurs in galvanostatic conditions.[35–37] Thus, expressions resulting under galvanostatic stimuli are useful for revealing actual electrodeposition phase transformations. They can analyse the nucleation process from electrodeposition under galvanostatic conditions directly, and another potentiostatic stimuli process is not necessary. Furthermore, *in situ* measurement can be achieved during galvanostatic stimuli electrodeposition.

We aimed to provide further insights into the nucleation process under galvanostatic stimuli to reveal electrochemical phase transformations during the early stages of electrodeposition. This work is based on the experimental data analysed by ohmic law during gold electrodeposition.

Specifications of the electrodeposition process

Three-dimensional nucleation controlled by diffusion generally involves several stages, either under potentiostatic or galvanostatic conditions. The schematic illustrations of the successive steps involved in electrodeposition[3,4] are shown in Fig. 1(a)–(d). The equivalent circuit between the cathode surface and reference electrode changed with the discharge steps as shown in Fig. 1(e)–(g).

With no extra-stimuli, the ion distribution is relatively random, as shown in Fig. 1(a). At the beginning of an extra-potential or extra-current stimulus, a crucial charging step for the electric double-layer capacitor occurred, and the distribution of ions became regular, as shown in Fig. 1(b). The equivalent circuit of this process was a resistor and a capacitor in series (RC), as shown in Fig. 1(e). As the electric double-layer capacitor charging proceeded, the overpotential of the double-layer was enough to motivate the ion discharge reaction. Then, ions diffused to the active point and discharged at the cathode surface. Nucleation and growth occurred at the same time, as shown in the schematic illustration in Fig. 1(c). The equivalent circuit of this process was two resistors and a capacitor in series (R(RC)), as shown in Fig. 1(f). During the nucleation and growth of deposits, the diffusion zones around the centre cannot provide enough ions to discharge, and the electrodeposition rate slows down with a diffusion-controlled process. The equivalent circuit contained two resistors, a capacitor and an inductance caused by diffusion, 'W', in series ($R(C(RW))$), as shown in Fig. 1(g). In this process, the diffusion region around each active point expanded, and an overlap region appeared, as shown in Fig. 1(d).

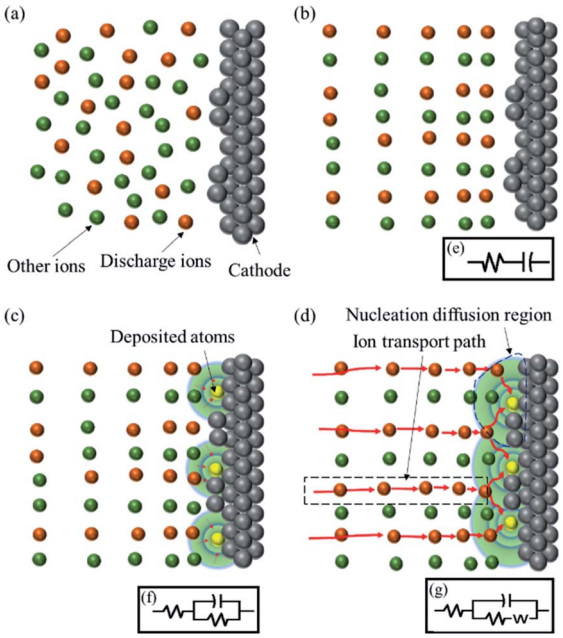

Fig. 1 Schematic illustration and equivalent circuit during electrodeposition nucleation at the early stage as controlled by diffusion; (a) no extra stimuli; (b) double-layer charging; (c) nucleation and growth; (d) diffusion-controlled process and diffusion region overlap; (e) double-layer charging equivalent circuit; (f) nucleation and growth equivalent circuit; (g) diffusion-controlled process equivalent circuit.

The abovementioned electrodeposition process is recognised widely. It is also the basis of electrodeposition research. The present work is also based on the above process and equivalent circuit. We aimed to provide further insight into the nucleation process under galvanostatic stimuli during early electrodeposition stages and calculate the potential transition function under galvanostatic stimuli.

Comparison of chronoamperometry and chronopotentiometry of gold electrodeposition using the SH model

The chronoamperometry curve of gold electrodeposition is shown in Fig. 2(a). The chronoamperometry curve can be

explained as before. At the beginning, there is charging current, which decays when charging is completed, as shown in the (*AB*) range. Then, electrodeposition nucleation occurred at point *B*. During nucleation, the electrodepositing current increases as the nuclei increase, either in terms of size or number, as presented in the (*BC*) range. During this stage of growth of the deposit, the mass transfer diffusion zone around each nucleus continuously extends. As the diffusion zone of a single nucleus expands, the hemispherical mass transfer diffusion zones of neighbouring nuclei overlap, and the diffusion zone transfers from hemispherical to cylindroid on the planar electrode, as shown in Fig. S1.† Then, the electrodeposition current falls, as planar infinite diffusion on the electrode surface extends to the depth of the solution gradually, shown as the (*CD*) range.

A similar changing rule was also found in the chronopotentiometry curve during gold electrodeposition, as shown in Fig. 2(b).

At the beginning, a double electrode layer charging process was observed. With double electrode layer charging, the electrode potential became more negative, and the electrode's overpotential increased with double layer charging, as shown in the (*ab*) range. When the overpotential value was sufficient for ion discharge, electrodeposition was activated, and nucleation occurred immediately. Along with nucleation and nuclear growth, the electroactive area on the electrode increased, and the impedance of the whole circuit decreased. Under constant current, the chronopotentiometry curve showed a downward trend, as revealed in the (*bc*) range. With the growth of each nucleus, the diffusion zones around the nuclei centres cannot provide enough ions to discharge, and the electrodeposition rate slowed down. The extra current was used to charge the double-layer capacitor. The overpotential then increased corresponding to double-layer charging,[24] as shown in the (*cd*) range, due to overlapping of the mass transfer diffusion zones.

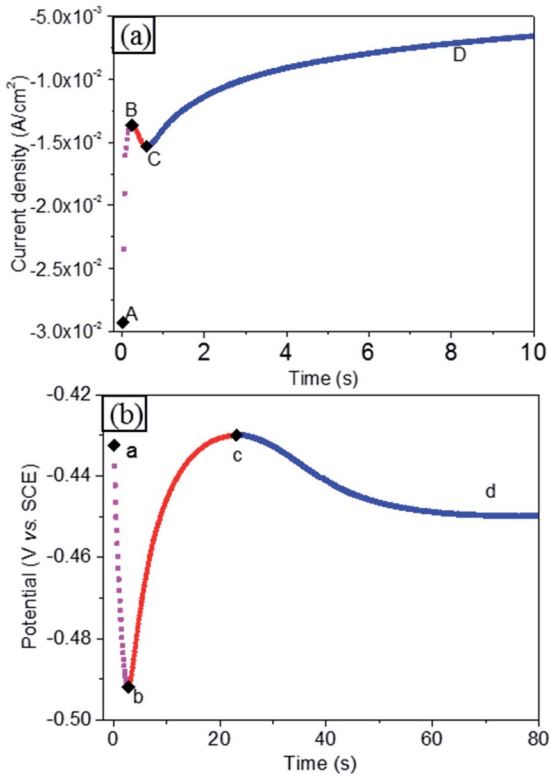

Fig. 2 Classical *i*–*t* and *E*–*t* curves during gold electrodeposition; (a) *i*–*t* curves; (b) *E*–*t* curves.

In summary, either the *i*–*t* curve under potentiostatic stimuli or *E*–*t* curve under galvanostatic stimuli reflected the same cathodic process. They also obeyed the equivalent circuit change, as shown in Fig. 1(e)–(f). Based on the analysis above, both the *i*–*t* curve and *E*–*t* curve can reflect the true electrodeposition process. Electrodeposition mostly occurred under the galvanostatic condition. Thus, developing non-dimensional plots from potentiostatic to galvanostatic is ideal and crucial to electrodeposition research. Next, we will prove that galvanostatic stimuli can be used to reveal that the nucleation process is viable.

The curve change analysis indicates that the *i*–*t* curve under potentiostatic stimuli and *E*–*t* curve under galvanostatic stimuli have opposite trends. For the same electrodeposition process, the increasing stage of the current curve corresponds to the decreasing stage of the potential curve. This phenomenon is in accordance with Ohm's law. The changes in current and voltage in the double electric layer on the cathode surface obey Ohm's law, indicating that the equivalent circuit can be used to analyse the correlation changes of the current and voltage during electrodeposition.

Before the analysis, we assumed that the impedance changes between the two electric layers were consistent in the electrodeposition process, either the *i*–*t* curve under potentiostatic stimuli or *E*–*t* curve under galvanostatic stimuli, according to the experimental process. The experimental tests reflect the same electrodeposition process.

On the theoretical side, the core of this study is the electrochemical phase transformations controlled by diffusion. In the diffusion-controlled electrodeposition, the whole electrochemical reaction is driven by the ion mass transformation instead of the electrochemical polarization. Thus, as reported by the SH model,[4] the reaction rate and the impedance values depend strongly on the ion mass transfer, but the effect of external polarization was not usually considered. Impedance, as a physical quantity representing the resistance of the circuit to the current, is determined by mass transfer of charged ions and the degree of discharge in the diffusion-controlled electrodeposition. Consequently, it is reasonable to assume that the electrochemical phase transformations and the impedance are independent of potential or current stimuli in the diffusion-controlled electrodeposition.

On the experimental side, Zhang Jie *et al.* presented a nucleation process of copper electrodeposition at varying potentials experimentally. Close scrutiny of their results revealed that the characteristics of continuous and instantaneous nucleation would not be obviously affected by the potential stimuli.[24] That is, the type of nucleation is determined by the bulk electrodeposition process; the experimental results are shown in Fig. S2.† In addition, the chronopotential curves for gold electrodeposition were plotted here (for details, see

Fig. S3†). These curves clearly revealed that the nucleation process of electrodeposition under different current or potential stimuli should be equivalent. At the same time, the trends of the *i*–*t* and *E*–*t* curves (shown in Fig. 2) also indicate that the impedance transformation influenced by the current is equal to the one caused by the potential stimuli. It should be noted that the uniform impedance transformation of the potential and current stimuli mentioned above has not been reported before to our best knowledge. Based on the analysis above, it is reasonable to assume that the impedance changes between the two electric layers are consistent in the electrodeposition process.

As such, the existing current transition formula and Ohm's law can be used to calculate the potential transition curve expression from potentiostatic mode. Next, we performed calculations based on the equation of current transformation obtained in the most typical SH model, as shown in eqn (3) and (4).

For a certain electrodeposition process under potentiostatic excitation, there is a corresponding galvanostatic excitation, which can produce the same electrodeposition process. We assumed that a corresponding i_0 can produce the same cathode deposition process with E_0.

The electrodeposition process shows the same impedance under either potentiostatic excitation or galvanostatic excitation. Thus, the impedance of the cathode deposition is equal at i_0 and E_0 stimuli. Thus, we can obtain the equation as follows:

The impedance under potentiostatic excitation is:

$$\text{Impedence} = E_0/I_t \tag{5}$$

The impedance under galvanostatic excitation is:

$$\text{Impedence} = \Delta E_T/I_0, \tag{6}$$

where ΔE_0 and I_t are the overpotential value and transient current under potentiostatic excitation and ΔE_T and I_0 are the transient overpotential value and current under galvanostatic excitation, respectively. ΔE_T and ΔE_0 are the potential values *versus* the electrode's steady potential.

Considering the same cathode deposition process, the impedance should be equal under galvanostatic excitation i_0 and potentiostatic excitation E_0, respectively.

Thus, the relationship is indicated by eqn (7).

$$\frac{\Delta E_0}{I_t} = \frac{\Delta E_T}{I_0} \tag{7}$$

Eqn (7) can be transformed to eqn (8) and (9).

$$I_t = \Delta E_0 \times I_0/\Delta E_T \tag{8}$$

$$\Delta E_T = \frac{\Delta E_0}{I_t \times I_0} \tag{9}$$

As previously indicated,[4] the current expression is presented as eqn (10).

$$I_t = \frac{zFD^{1/2}c\theta}{\pi^{1/2}t^{1/2}}, \tag{10}$$

where D is the diffusion coefficient, c is the bulk concentration, zF is the molar charge of the electrodepositing species and θ is the actual fraction of mass transfer diffusion area covered considering the overlap. Combining eqn (8) and (10)), the following relationship can be obtained, as shown in eqn (11).

$$\Delta E_0 \times \frac{I_0}{\Delta E_T} = I_t = \frac{zFD^{1/2}c\theta}{\pi^{1/2}t^{1/2}} \tag{11}$$

From previous analysis,[4] there was a maximum value of nucleation current under potentiostatic stimuli. Analysis of the chronoamperometry and chronopotentiometry curves indicates a minimum value of nucleation overpotential under galvanostatic stimuli. Meanwhile, the maximum and minimum values are respectively observed from the *E*–*t* and *i*–*t* curves in Fig. 2. Thus, the non-dimensional plots can be transmitted into eqn (12).

$$\left(\frac{I_t}{I_{max}}\right)^2 = \frac{(\Delta E_0 \times I_0/\Delta E_T)^2}{(\Delta E_0 \times I_0/\Delta E_{min})^2} = \left(\frac{\Delta E_{min}}{\Delta E_T}\right)^2 \tag{12}$$

Thus, $\left(\frac{\Delta E_{min}}{\Delta E_T}\right)^2$ shows the same trend as $\left(\frac{I_t}{I_{max}}\right)^2$.

The quantitative characterization of the potential drop across the double layer in diffusion-controlled electrodeposition has not been reported before to our best knowledge. The correlation between ion transport and the current transformation has been reported previously, as summarized in Table S1.† As shown in Table S1,† it is clear that during diffusion-controlled electrodeposition, ion mass transfer has been widely used to calculate the current transformation. According to eqn (12), it enables us to reveal the role of potential transformation based on the current transformation results. Note that this is a new viewpoint and has not been reported before.

For instantaneous nucleation, N is the number of centres instantaneously nucleated per unit area at $t = 0$, and for progressive nucleation, the number of centres nucleated per unit area at t, $N_{(t)} = AN_m t$, where A is the nucleation rate per active site in eqn (1) and (2). Indeed, the values of these parameters were different at varying stimuli conditions. For example, the N values changed with varying potential (all raw data are given in Table S2†). Because the N value changed with varying potential E or current I, the quality of the electrodeposited film can be adjusted by changing E or I.

However, the data calculated in eqn (3) and (4) obtained by solving the function are not closely related to the change of A, N and N_m values. The systematic calculation has been explained in ESI† part 1. Though the parameter values change at varying stimuli conditions, it is noteworthy that the nuclear species remain unchanged regardless of instantaneous or progressive nucleation.

Based on the calculation, a group of non-dimensional expressions can be obtained for instantaneous and

progressive nucleation under galvanostatic conditions from eqn (3) and (4).

For instantaneous nucleation:

$$\left(\frac{\Delta E_{\min}}{\Delta E_{\mathrm{T}}}\right)^2 = \left(\frac{I_{\mathrm{t}}}{I_{\max}}\right)^2 = \frac{1.9542}{t/t_{\mathrm{m}}}\{1-\exp[-1.2564(t/t_{\mathrm{m}})]\}^2, \quad (13)$$

For progressive nucleation:

$$\left(\frac{\Delta E_{\min}}{\Delta E_{\mathrm{T}}}\right)^2 = \left(\frac{I_{\mathrm{t}}}{I_{\max}}\right)^2 = \frac{1.2254}{t/t_{\mathrm{m}}}\left\{1-\exp\left[-2.3367(t/t_{\mathrm{m}})^2\right]\right\}^2, \quad (14)$$

where $\Delta E_{\min}$ corresponds to the minimum polarisation value and can be calculated by equating the derivative of the E–t curve to zero. With the above changes, the time t_{m} will be changed from the original t_{m} corresponding to the maximum current to the time t_{m} corresponding to the minimum polarisation value.

For each electrodeposition, ion mass transfer and the impedance usually keep constant. Based on the analysis above, it is easy to find that the time (t_{m}) of maximum current ($I_{\max}$), as well as the time(t_{m}) of minimum potential ($\Delta E_{\min}$) under potentiostatic stimuli is a critical state of the single nuclear diffusion region for mass-transfer. The critical state is the emergence of overlap (as shown in Fig. S1†). Comparing the impedance before and after the emergence of overlap, it is easy to find that the impedance gradually decreases, then increases and finally levels off. Intrinsically, the two extreme values—$I_{\max}$ and $\Delta E_{\min}$—are considered to be equal to the impedance of a minimum (or the emergence of overlap) in the diffusion-controlled electrodeposition. In other words, the actual time that two extreme values appear is the moment that the overlap emerges. In addition, according to Faraday's law, eqn (5) and (6) showed that E was inversely proportional to I. Thus, for a maximum ($I_{\max}$) under potentiostatic stimuli, there will be a minimum ($\Delta E_{\min}$) under galvanostatic stimuli.

As such, this work proved and provided non-dimensional expressions for instantaneous and progressive nucleation under galvanostatic stimuli. Eqn (13) and (14) are similar to the non-dimensional expressions under potentiostatic conditions in the SH model; however, the electrodepositing nucleation under galvanostatic conditions should be investigated directly. Eqn (13) and (14) can provide *in situ* testing for the widely used galvanostatic electrodeposition process.

The non-dimensional expressions eqn (13) and (14) for instantaneous and progressive nucleation under galvanostatic stimuli were validated using chronoamperometry and chronopotentiometry curves during gold electrodeposition on a Cu substrate. The detailed experimental test process was similar to a previous work,[33] as explained in ESI† part 2.

The chronopotentiometry curves at various current stimuli are shown in Fig. 3. These two curves reflect that a charging process is present at the beginning. The overpotential increased as charging proceeded. When the overpotential value was sufficient for gold ion discharge, an electrodeposition stage occurred. During nucleation and growth, the succeeding curve shows an upswing trend, reflecting the decrease in impedance and overpotential, with the electrodeposition area expanding, either in terms of size or number. With the growth of nuclei, the diffusion zones around each nucleus cannot provide enough ions for discharge. Therefore, the electrodeposition rate slowed down, and the extra current will be used to charge the double-layer capacitor. The overpotential then increased corresponding to linear diffusion. This process is the same as that described in Fig. 2(a) and (b), before.

Thus, eqn (13) and (14) were used to analyse the chronopotentiometry curves (Fig. 3). The non-dimensional expressions of the SH model[4] are also employed to analyse the current transients measured in comparison. The nucleation mechanism models proposed by Scharifker and Hills (SH model) are famous and widely used in many reported theoretical models of nucleation mechanisms.

Chronopotentiometry curves were transformed into non-dimensional plots of $(E_{\min}/E_{\mathrm{t}})^2$ *versus* (t/t_{m}), and the plots were compared with non-dimensional transient curves and $(I/I_{\mathrm{m}})^2$ *versus* (t/t_{m}) curves under potentiostatic conditions (Fig. 4).

The $(I/I_{\mathrm{m}})^2 - (t/t_{\mathrm{m}})$ curve (the curve marked with a black box in Fig. 4) transformed by the SH model is taken as a reference, because the model is used as the basis for this study. Note that the SH model is a well-known equation and has been extensively verified. The $(I/I_{\mathrm{m}})^2 - (t/t_{\mathrm{m}})$ curve shows the role of the instantaneous nucleation during gold deposition in DMH-containing electrolyte. At the same time, careful inspection of Fig. 4 reveals that the converse E–t curves obtained at 0.0125A cm^{-2} and 0.025A cm^{-2} (galvanostatic stimuli) based on the formula proposed in this paper also show the characteristics of instantaneous nuclear growth. The results above led to an interesting finding that chronoamperometry measurement in the SH model works equally well for the chronopotentiometry measurement developed in this paper.

In addition, it is easy to find that, for $0 < t/t_{\mathrm{m}} < 2$, three experimental curves largely follow the theoretical instantaneous nucleation curve; for $t/t_{\mathrm{m}} > 2$, the trend in the change of the three experimental curves is quite different from that of the theoretical instantaneous nucleation curves. It has been reported that extra reaction[29] and limited diffusion[32] should be the probable cause for the deviation of the experimental curves

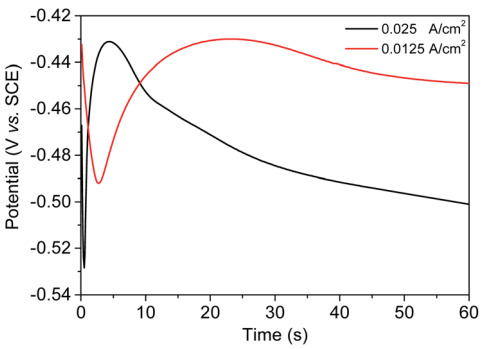

Fig. 3 E–t curves at various current stimuli.

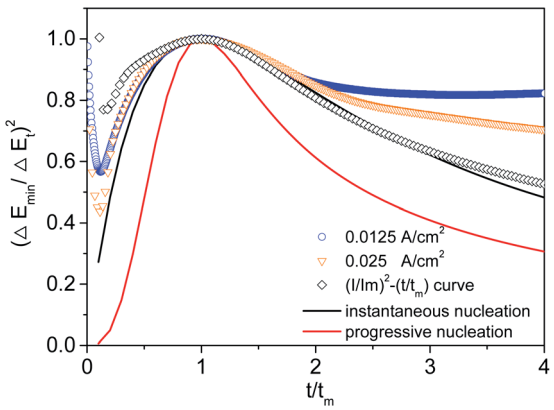

Fig. 4 Experimental analysis using $(\Delta E_{min}/\Delta E_T)^2$ *versus* t/t_m non-dimensional plots.

at larger t/t_m. Moreover, this finding has been fully discussed in our previous paper[33] in terms of limited-diffusion mass transfer (for details see ESI† part 3).

Chronopotentiometry and chronoamperometry curves have the same trend after transformation. The transformation curve revealed that gold nucleation in the electrolyte was instantaneous.

This phenomenon indicates that the potential curve calculated under galvanostatic conditions can also effectively analyse the nucleation process of electrodeposition. The test results were consistent with theoretical analysis and formula derivation. It also demonstrated that chronopotentiometry curves from galvanostatic stimuli are an effective method to reveal the phase transformations in early electroplating stages.

Summary

This work provides a new insight into the early stages of electrodeposition from galvanostatic stimuli rather than the widely used potentiostatic conditions at present, from theoretical and experimental aspects. With theoretical Ohm's law electro-relationship formula derivation, we found a similar relationship between $(\Delta E_{min}/\Delta E_T)^2$, $(I_t/I_{max})^2$ and t/t_m. The relationship between $(\Delta E_{min}/\Delta E_T)^2$ and t/t_m provides a direct method of investigating the nucleation process during galvanostatic electrodeposition. On the basis of the theoretical calculations, gold electrodeposition was analysed using eqn (13) and (14), and the SH model eqn (1) and (2) were obtained. An equivalent conclusion was found between the non-dimensional expressions for instantaneous and progressive nucleation under galvanostatic stimuli as proven in the present work and the SH model. In summary, this work provides a new, convenient and direct method of investigating the nucleation process during electrodeposition.

Conflicts of interest

There are no conflicts to declare.

Acknowledgements

This study was performed with the support of the fund "Research Project of Guangdong University of Petrochemical Technology, 2019rc069" and "Science and Technology Program of Maoming, 2021019".

References

1 E. Budevski, G. Staikov and W. J. Lorenz, *Electrochim. Acta*, 2000, **45**(15), 2559.
2 P. Altimari and F. Pagnanelli, *Electrochim. Acta*, 2016, **205**, 113.
3 M. E. Hyde and R. G. Compton, *J. Electroanal. Chem.*, 2003, **549**(1), 1.
4 B. Scharifker and G. Hills, *Electrochim. Acta*, 1983, **28**(7), 879.
5 E. Budevski, *Prog. Surf. Membr. Sci.*, 1976, **11**, 71.
6 M. Avrami, *J. Chem. Phys.*, 1939, **7**(12), 1103.
7 S. Rangarajan, *J. Electroanal. Chem. Interfacial Electrochem.*, 1973, **46**(1), 125.
8 R. Armstrong, M. Fleischmann and H. Thirsk, *J. Electroanal. Chem.*, 1966, **11**(3), 208.
9 E. Bosco and S. Rangarajan, *J. Electroanal. Chem. Interfacial Electrochem.*, 1982, **134**(2), 213–224.
10 E. Bosco and S. Rangarajan, *J. Electroanal. Chem. Interfacial Electrochem.*, 1982, **134**(2), 225.
11 G. J. Hills, D. J. Schiffrin and J. Thompson, *Electrochim. Acta*, 1974, **19**(11), 657.
12 G. A. Gunawardena, G. J. Hills and I. Montenegro, *Electrochim. Acta*, 1978, **23**(8), 693.
13 G. Hills, I. Montenegro, B. Scharifker, F. Palmisano, E. Desimoni, L. Sabbatini, G. Torsi and P. G. Zambonin, *J. Appl. Electrochem.*, 1980, **10**(6), 807.
14 G. Hills, A. K. Pour and B. Scharifker, *Electrochim. Acta*, 1983, **28**(7), 891.
15 G. Hills, D. Schiffrin and J. Thompson, *Electrochim. Acta*, 1974, **19**(11), 657.
16 G. Hills, D. Schiffrin and J. Thompson, *Electrochim. Acta*, 1974, **19**(11), 671.
17 J. Ustarroz, X. Ke, A. Hubin, S. Bals and H. Terryn, *J. Phys. Chem. C*, 2012, **116**(3), 2322.
18 M. Huynh, D. K. Bediako, Y. Liu and D. G. Nocera, *J. Phys. Chem. C*, 2014, **118**(30), 17142.
19 H. Liu, F. Favier, K. Ng, M. P. Zach and R. M. Penner, *Electrochim. Acta*, 2001, **47**(5), 671.
20 W. Schmickler, K. Pötting and M. Mariscal, *Chem. Phys.*, 2006, **320**(320), 149.
21 X. Ren, Y. Song, A. Liu, J. Zhang, P. Yang, J. Zhang and M. An, *RSC Adv.*, 2015, **5**(80), 64997.
22 X. Ren, Y. Song, A. Liu, J. Zhang, G. Yuan, P. Yang, J. Zhang, M. An, D. Matera and G. Wu, *Electrochim. Acta*, 2015, **176**, 10.
23 T. Vitanov, A. Popov, G. Staikov, E. Budevski, W. J. Lorenz and E. Schmidt, *Electrochim. Acta*, 1986, **31**(8), 981.
24 J. Zhang, A. Liu, X. Ren, J. Zhang, P. Yang and M. An, *RSC Adv.*, 2014, **4**(72), 38012.
25 F. C. Walsh and C. T. J. Low, *Surf. Coat. Technol.*, 2016, **288**, 79.

26 Z. Feng, Q. Li, J. Zhang, P. Yang, H. Song and M. An, *Surf. Coat. Technol.*, 2015, **270**, 47.
27 D. Kong, Z. Zheng, F. Meng, N. Li and D. Li, *J. Electrochem. Soc.*, 2018, **165**(16), D783.
28 M. Palomar-Pardavé, B. R. Scharifker, E. M. Arce and M. Romero-Romo, *Electrochim. Acta*, 2005, **50**(24), 4736.
29 B. R. Scharifker and J. Mostany, *J. Electroanal. Chem.*, 1984, **177**, 13.
30 L. Heerman and A. Tarallo, *Electrochem. Commun.*, 2000, **2**(2), 85.
31 P. Altimari, F. Greco and F. Pagnanelli, *Electrochim. Acta*, 2019, **296**, 82.
32 P. C. T. D'Ajello, M. L. Munford and A. A. Pasa, *J. Chem. Phys.*, 1999, **111**(9), 4267.
33 G. Luo, D. Li, G. Yuan and N. Li, *J. Electrochem. Soc.*, 2018, **165**(3), D147.
34 N. Reim, A. Littig, D. Behn and A. Mews, *J. Am. Chem. Soc.*, 2013, **135**(49), 18520.
35 X. F. Ren, Y. Song, A. M. Liu, J. Zhang, P. X. Yang, J. Q. Zhang, G. H. Yuan, M. Z. An, H. Osgood and G. Wu, *RSC Adv.*, 2015, **5**(79), 64806.
36 A. Liu, X. Ren, B. Wang, J. Zhang, P. Yang, J. Zhang and M. An, *RSC Adv.*, 2014, **4**(77), 40930.
37 G. Luo, G. Yuan and N. Li, *RSC Adv.*, 2016, **6**(66), 61341.